Available online at www.sciencedirect.com
ScienceDirect
Acta Materialia 58 (2010) 5420–5432
Acta MATERIALIA
www.elsevier.com/locate/actamat

Plastic deformability of metallic glass by artificial macroscopic notches

J.X. Zhao [a], F.F. Wu [a,b], R.T. Qu [a], S.X. Li [a], Z.F. Zhang [a,*]

[a] *Shenyang National Laboratory for Materials Science, Institute of Metal Research, Chinese Academy of Sciences, 72 Wenhua Road, Shenyang 110016, China*

[b] *School of Materials Science and Engineering, Liaoning University of Technology, 169 Shiying Street, Jinzhou 121001, China*

Received 23 March 2010; received in revised form 6 June 2010; accepted 8 June 2010
Available online 10 July 2010

Abstract

This paper reports that the plasticity of Zr-based metallic glass can be improved by creating two symmetrical semi-circular notches. Unlike the experimental findings of the samples without notches, a steady shear deformation can be created by the large-scale stress gradient around the two symmetrical notches and the plasticity of metallic glass can be enhanced to a high value of ~10% under compression tests. The improved plasticity may be due to the easy initiation of shear bands around the notches, and the consequent blocking effect of notches on the propagation of shear bands, similar to the dislocation mechanism in crystalline materials. To reveal the particular plastic deformation behavior of metallic glass, Ti_3SiC_2 ceramic and high-strength steel specimens with two symmetrical semi-circular notches were also conducted under compressive loadings; however, no enhancement in plasticity was found. It is suggested that creating a stress gradient is a particular strategy for designing metallic glasses in order to improve their plasticity.

Keywords: Metallic glass; Shear band; Plastic deformation; Notch; Stress gradient

1. Introduction

Metallic glasses have received much attention due to their mechanical properties, such as high strength and high hardness, which are attractive in structural materials [1–10]. Under tensile and compressive loadings, metallic glasses may fail along one main shear band (SB) and display near zero plasticity [11–17]. This low plasticity has limited the engineering application of metallic glasses and many different ways to improve their plastic deformation abilities have been tried. In general, two different approaches have been utilized to enhance the plasticity of metallic glasses. (i) Some metallic glassy composites have been fabricated so as to improve their plasticity [18,19], e.g. adding secondary-phase particles or high-strength fibres to the amorphous alloys [20,21], or preparing metallic glassy composites containing in situ formed ductile dendrites [22]. It was found that the reinforced phases can restrain the rapid propagation of SBs and change the direction of extension thereby improving the plasticity. Additionally, a number of approaches have verified that the correlation between mechanical properties and elastic modulus demonstrates that brittleness in metallic glasses can be alleviated by alloying some elements with low μ/B (or, equivalently, high υ) as constituents [23,24]. (ii) It was found that sufficient SBs were formed to accommodate the high plasticity when the aspect ratio of the compressive specimens was smaller than 1.0 [25–29]. Recently, by processing one layer on the surface of a metallic glass after shot peening, considerable plasticity could also be obtained in Zr-based metallic glass [30]. Moreover, it was reported that the plasticity of metallic glasses can be efficiently enhanced due to the confined loadings either by application of Cu plating [31] or by using a

* Corresponding author. Tel.: +86 24 23971043; fax: +86 24 23891320.
E-mail address: zhfzhang@imr.ac.cn (Z.F. Zhang).

1359-6454/$36.00 © 2010 Acta Materialia Inc. Published by Elsevier Ltd. All rights reserved.
doi:10.1016/j.actamat.2010.06.017

confining sleeve technique [32] in the metallic glasses. In addition, the small punch test (SPT) was also found to be an effective method of stimulating more SBs under multiaxial loading [33,34], and the related findings demonstrated that metallic glass could be controlled to create regular arranged fine multiple SBs with a large plastic strain (19.6%) [34].

For crystalline materials, the dislocations and slip systems are the key factors controlling the plastic deformation behavior [35]. As schematically shown in Fig. 1a, under tensile loading, it is well known that the whisker has extremely high yield strength but fails with low plasticity [36]. However, for ductile single crystals, due to the existence of dislocations, the local region first yields quite easily at a much lower stress. Furthermore, the dislocations can move along the slip planes easily and interact with each other. Meanwhile, as illustrated in Fig. 1b, the interactions and multiplications of the abundant dislocations contribute to the work-hardening and super-high plastic deformation abilities [35]. Normally, the typical tensile stress–strain curves of whisker and bulk single crystals can be illustrated as in Fig. 1c [35–38]; the large difference in the two tensile stress–strain curves can be explained by the existence of mobile dislocations, which can greatly decrease the yield strength of single crystals, while their consequent interactions and multiplications may enhance the plasticity to a large extent [35].

In contrast to crystalline materials, for metallic glasses without lattice dislocations and slip systems, shear banding becomes the significant plastic deformation mechanism [11]. Once yielding starts, the SBs propagate rapidly, resulting in a catastrophic fracture [11–17]. Hypothetically, can the metallic glasses also display a large plasticity by artificially inducing some defects which play a role similar to that played by dislocations in the crystalline materials? That is to say, if the SBs in metallic glasses initiate easily and expand with difficulty when stimulated by artificial defects, the entire plasticity can also be greatly enhanced. Such a strategy would, if realized, exploit the essential deformation mechanism of metallic glasses. Therefore, to obtain a similar deformation mechanism in metallic glasses, in the present work, we conducted a series of compression experiments on a Zr-based metallic glass containing the following two design aspects. Firstly, in order to make the SBs in metallic glass initiate at a lower stress level like slip dislocations in crystals [35], we created notches in the specimen so that the metallic glass samples can yield easily around notch at a lower stress level. Secondly, in order to achieve SB interactions, we created semi-circular notches at different positions along the edge of samples as well as a circular hole in the middle of the sample. In this situation, the different stress gradients might bring about SB interactions and greatly improve the plasticity. Compared with the unnotched samples, the plasticity of the metallic glass with two semi-circular symmetrical notches can be increased by up to ~10%; however, the nominal yield strength only decreases about 17%. The current results demonstrate that the interactions of SBs induced by the artificial defects may provide some new understanding on the plastic deformation mechanism of metallic glasses rather than the improved plasticity itself.

2. Experimental procedures

Zr-based metallic glass plates with a nominal chemical composition of $Zr_{52.5}Ni_{14.6}Al_{10}Cu_{17.9}Ti_5$ were prepared by arc-melting. The final plate had a rectangular shape, with dimensions of $60 \times 30 \times 3\ mm^3$. The microstructure of the as-cast specimens was characterized by scanning electron microscopy (SEM) using a Leo Supra 35, as well as by X-ray diffraction (XRD) using a Rigaku X-ray diffractometer with Cu $K\alpha$ radiation. XRD patterns demonstrate that the as-cast Zr-based metallic glass has a fully amorphous structure. As illustrated in Fig. 2, the metallic glass plates were cut into five specimens defined as A–E with dimensions of $3.0 \times 3.0 \times 6.0\ mm^3$, and the semi-circular notches, as well as the circular hole, all have a radius of 0.5 mm. The positions of the semi-circular notches and hole are also displayed in Fig. 2. Conventional compression tests were conducted to measure the mechanical

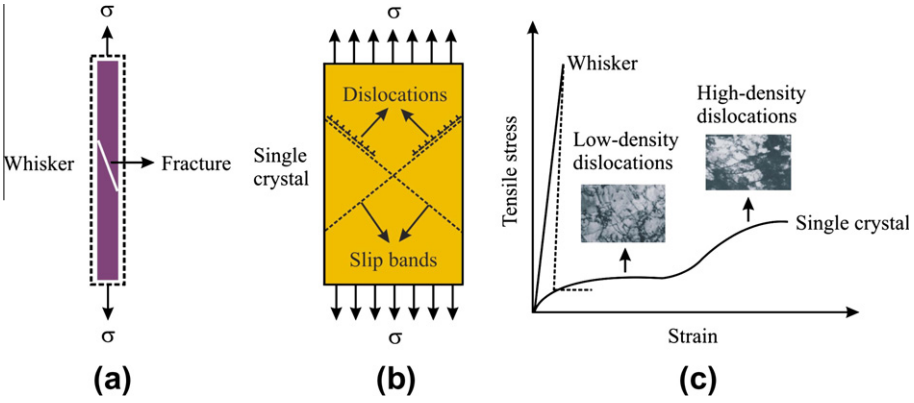

Fig. 1. (a) Illustration of tensile deformation mechanism for a whisker [36]; (b) interactions of dislocations on slip planes for a single crystal; (c) illustration of tensile stress–strain curves of whisker and single crystal [35–38].

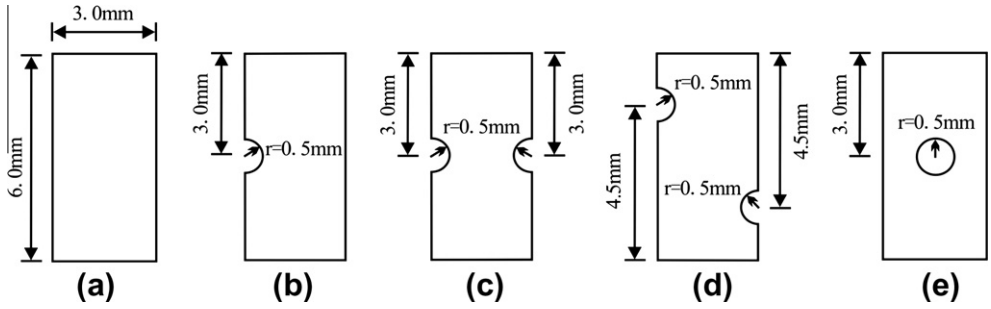

Fig. 2. Illustration of five kinds of specimens under compression tests. The related dimensions are marked.

properties of the metallic glass specimens with an MTS810 testing machine at room temperature in air. All the tests were conducted using a constant strain rate of $10^{-4}\ s^{-1}$. After the tests, all the specimens were observed by SEM to reveal the deformation and fracture features. In addition, theoretical analysis and finite-element method (FEM) with the software code ANSYS were used for resolving and simulating the stress distribution of the different specimens.

3. Experimental results

3.1. Nominal compressive stress–strain responses

It is well known that the stress distributions in notched specimens are highly complex due to the existence of stress raisers such as notches or holes. In order to compare the stress–strain curves of the notched and unnotched specimens and to obtain the global plasticity of these samples, we defined the nominal stress to represent the global stress in a specimen by selecting the area of the both unnotched and notched specimen end as the nominal area. In this case, the area is about $3.0 \times 3.0\ mm^2$. In this way, the strength and global plasticity for the five samples A–E in Fig. 2 can be compared with each other by a uniform standard. Here, the stress and strain are referred to as "nominal" instead of "engineering".

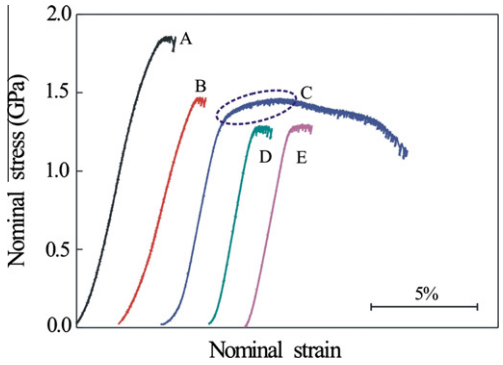

Fig. 3. Nominal compressive stress–strain curves for the five Zr-based metallic glass specimens A–E.

In Fig. 3, the nominal compressive stress–strain curves for the specimens A–E are displayed. Curve A, which represents the sample without notches, shows only a little plasticity (about 0.5%) with a yield strength of ~1.80 GPa [11,39]. Similar plasticity (about 0.5–1.0%) was obtained for curve B (the nominal yield strength is ~1.50 GPa) and curve D (the nominal yield strength is ~1.25 GPa) with one notch or two asymmetric notches. For the sample with one hole (specimen E), the nominal yield strength fell to 1.25 GPa, while the plasticity is only 1.0%, which is slightly larger than the situation without the hole [11,39]. However, a relatively high plasticity (~10%) was found in sample C with two symmetrical notches, accompanying by a stress increasing stage (marked as elliptical dotted line) and a nominal yield strength of ~1.50 GPa.

Obviously, the decline in the nominal yield strength and the large plasticity enhancement displayed in specimen C in Fig. 3 are similar to the features in crystalline materials [35] (see Fig. 1c), and quite different to those obtained by conventional compression tests on the identical Zr-based metallic glass [39], implying that a deeper understanding of this plastic deformation mechanism of metallic glass is required.

3.2. Plastic deformation behaviors

Figs. 4 and 5 show SEM images of deformation features corresponding to the samples A–E in Fig. 2. It can be seen that the specimens, except for sample C, were conventionally split into two parts along major SBs [11,39,40]. Their shear fracture angles are about 41°, which is consistent with the results from uniaxial compression tests [11,39,40]. However, specimen C did not break apart even when the plastic strain had reached ~10%; instead, a V-shaped shear region appeared around the notches with the shear angle of about 40°. From Fig. 4c, it seems that the SBs appeared first on the notch regions and then expanded into two major SBs, which then intersected with each other and had an out-of-plane displacement.

Additionally, in order to describe the microcosmic shear deformation behavior, magnified images of regions I–VIII marked in Fig. 4 are shown in Fig. 5. In region I, some SBs are found to rotate at the edge of the specimen A,

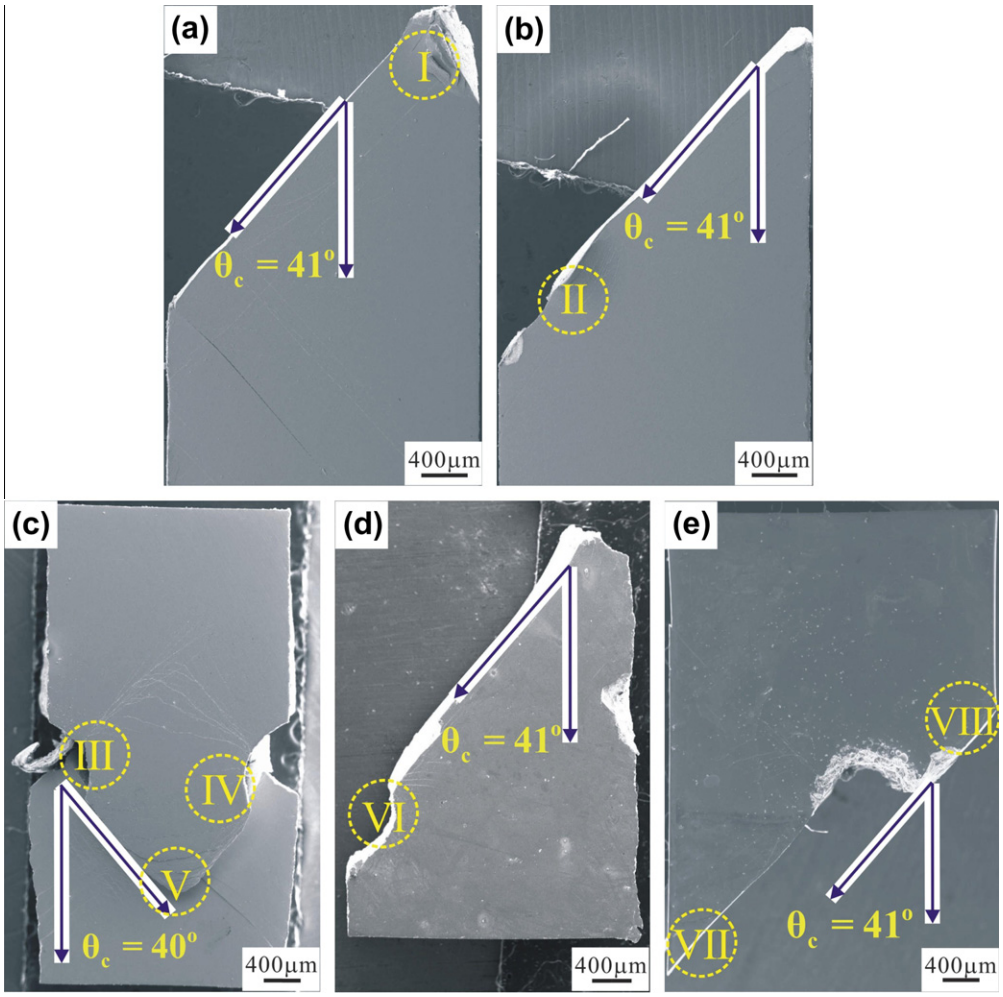

Fig. 4. SEM images on the deformation and fracture morphologies of specimens A–E shown in Fig. 3. (a) Specimen without notches; (b) specimen with one notch; (c) specimen with two symmetrical notches; (d) specimen with two asymmetrical notches; (e) specimen with one circular hole. Additionally, eight regions marked I–VIII are selected for further observation.

implying that the fast propagation of the major SB might be hindered, resulting in a small plasticity [11,39], as displayed in Figs. 4a and 5a. For region II in specimen B, as shown in Figs. 4b and 5b, however, some tiny SBs were found to appear around the semi-circular notches; these SBs could also confine the rapid extension of the major SB and increase the plasticity to a far lesser extent. Fig. 5c–e show the magnified images indicated in Fig. 4c for specimen C. As shown in Fig. 5c and d, near to the notches, in regions III and IV respectively, large shear deformation takes place around the notches primarily because of the stress concentration around notches. In region V displayed in Fig. 5e, however, two major SBs intersect into one point and there is an out-of-plane displacement with many tiny SBs on the tip of a V-shaped extrusive region, indicating that the intersection of the two major SBs can result in an increase of strength and also improve the plasticity (near to ~10%, shown in Fig. 3), just as the dislocation interaction do [35–38]. Fig. 5f shows an SEM image of specimen D; it is also found that only a few short SBs appeared around the notch (region VI). In the meantime, according to Fig. 4d, it can be concluded that the initial SBs appeared first around two notches with parallel extension directions and finally rolled into one major SB. Moreover, for the sample with a hole in middle, two regions (VII, VIII) were selected to reveal the microscopic shear behaviors, as shown in Figs. 4e and 5g and h. It is found that only very few tiny SBs appeared on the two regions around the major SBs which were caused by the fracture process [11,39,40].

In brief, compared with the above results of the specimens with the notches and hole, specimen C can display a larger plasticity, in which the specimen did not break into two parts even though the plasticity had reached ~10%. Therefore, installing two symmetrical notches might provide a new design method for improving the plasticity of metallic glass. More important, this particular mechanism may help us to understand the plastic deformation ability of metallic glass by introducing the stress gradient.

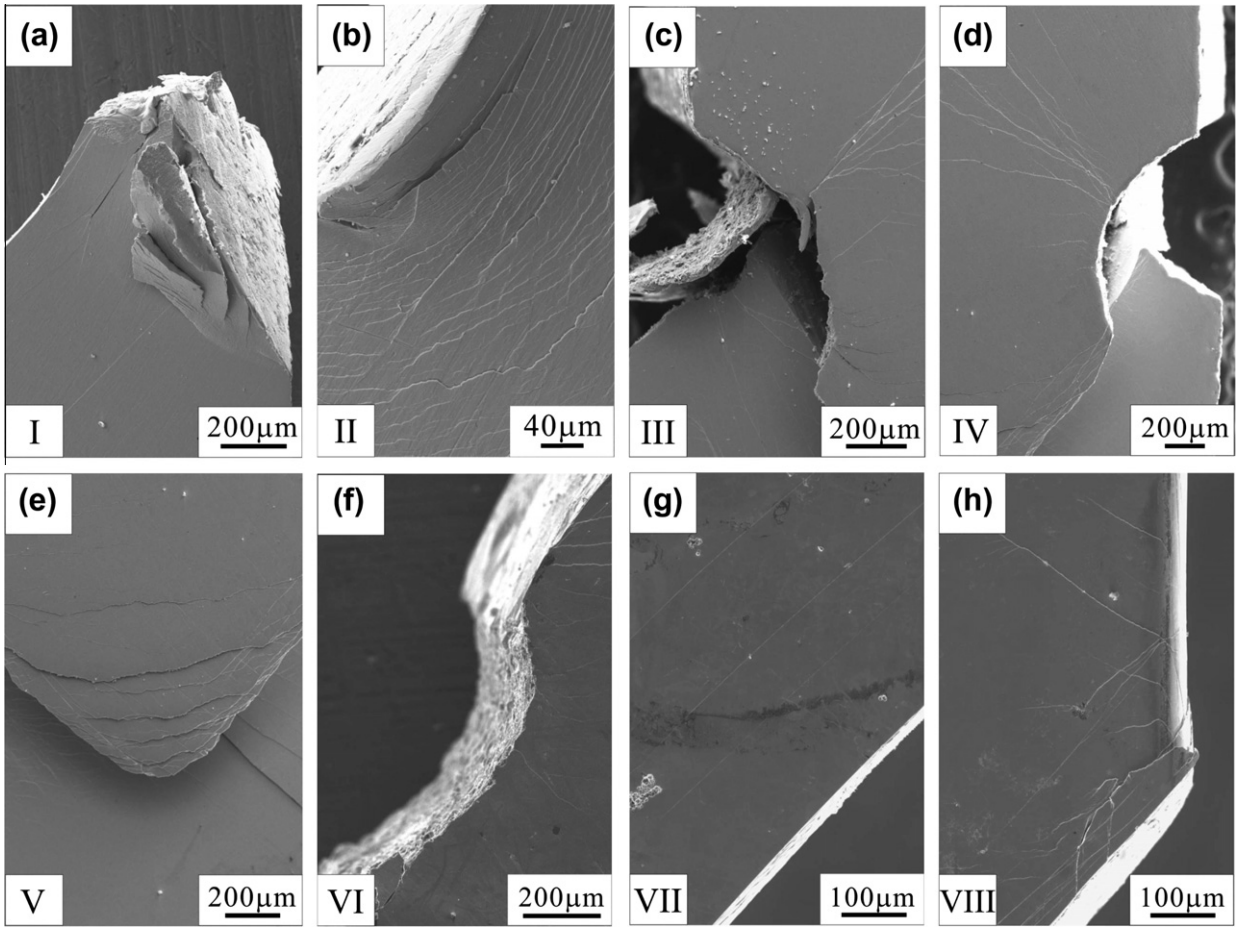

Fig. 5. Microscopic images observed by SEM for the selected regions in Fig. 4a–h correspond with regions I–VIII.

4. Discussion

4.1. Theoretical analysis

It is well known that the structure of metallic glasses is disordered; therefore, metallic glass can be considered, at least on the macro-scale, as an ideal model material with isotropic structure [41]. Therefore, we can obtain some semiquantitative understanding of the effects of notches through elastic mechanics. The mechanical problems induced by notches or holes have been investigated by several researchers [42–48]; metallic glass specimens with notches have been researched experimentally [47,48]. In the following sections, elastic analytical solutions [43,44] and approximate expressions [45] are adopted to provide some estimates for the stress distribution and reduction in yield strength for notched samples.

4.1.1. Stress distribution around the notches or the hole

In this section, the method used by Fillippi et al. [44] is employed to study the stress concentration caused by one notch. As shown in Fig. 6a, in polar coordinates (ρ, θ), a semi-infinite plate with one semi-circular notch of radius ρ_0 under compression loadings is illustrated. Based on the elastic mechanics solution [44], the stress components σ_θ, σ_ρ, $\tau_{\rho\theta}$ can be expressed as:

$$\begin{Bmatrix}\sigma_\theta\\ \sigma_\rho\\ \tau_{\rho\theta}\end{Bmatrix} = \lambda_1\rho^{\lambda_1-1}a_1\left[\begin{Bmatrix}(1+\lambda_1)\cos(1-\lambda_1)\theta\\ (3-\lambda_1)\cos(1-\lambda_1)\theta\\ (1-\lambda_1)\sin(1-\lambda_1)\theta\end{Bmatrix} + \chi_{b1}(1-\lambda_1)\begin{Bmatrix}\cos(1+\lambda_1)\theta\\ -\cos(1+\lambda_1)\theta\\ \sin(1+\lambda_1)\theta\end{Bmatrix} + \frac{q}{4(q-1)}\left(\frac{\rho}{\rho_0}\right)^{\mu_1-\lambda_1}\left(\chi_{d1}\begin{Bmatrix}(1+\mu_1)\cos(1-\mu_1)\theta\\ (3-\mu_1)\cos(1-\mu_1)\theta\\ (1-\mu_1)\sin(1-\mu_1)\theta\end{Bmatrix} + \chi_{c1}\begin{Bmatrix}\cos(1+\mu_1)\theta\\ -\cos(1+\mu_1)\theta\\ \sin(1+\mu_1)\theta\end{Bmatrix}\right)\right] \quad (1)$$

$$a_1 = \frac{\sigma_{max}}{\lambda_1\rho_0^{\lambda_1-1}(1+\lambda_1+\chi_{b1}(1-\lambda_1)+[(1+\mu_1)\chi_{d1}+\chi_{c1}]\{q/4(q-1)\})} \quad (2)$$

For the semi-circular notch, the coefficients can be determined as follows [44]:

$$\lambda_1 = 0.5,\ \mu_1 = -0.5,\ \chi_{b1} = 1.0,\ \chi_{c1} = 4.0,\ \chi_{d1} = 0.0,\ q = 2.0, \quad (3)$$

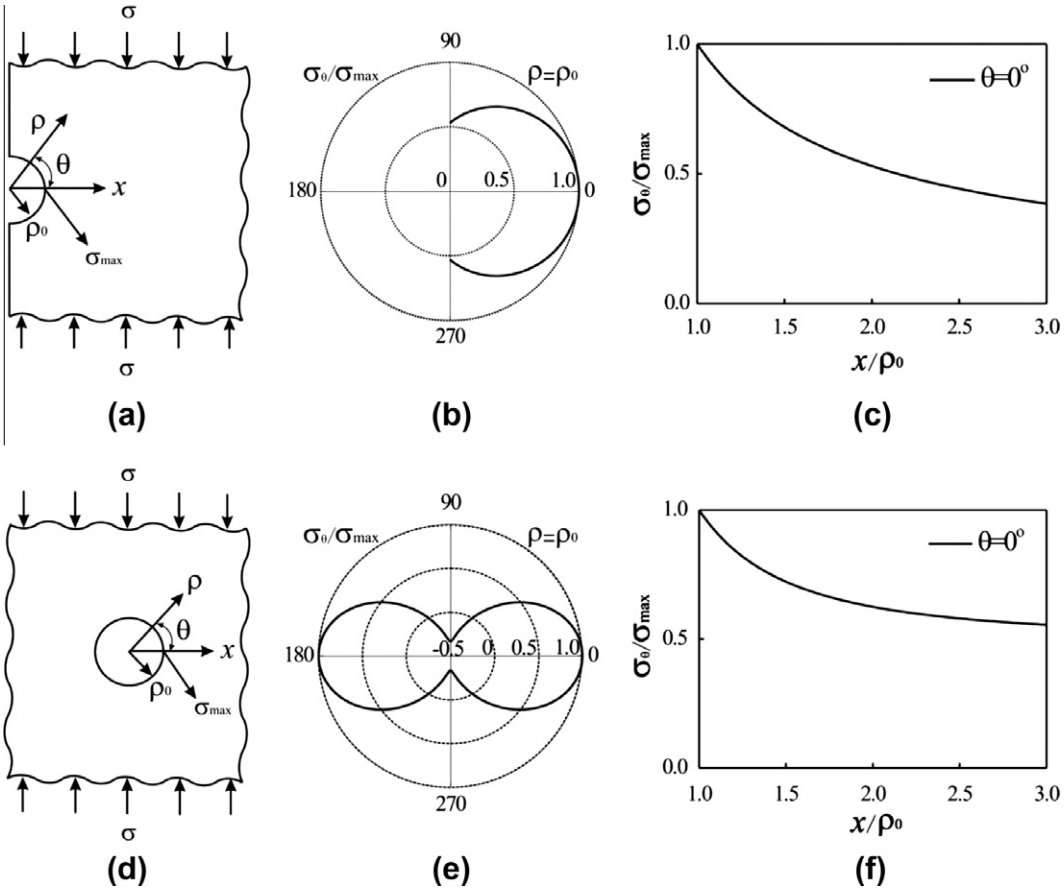

Fig. 6. Theoretical analysis on the stress concentration problems caused by one notch or a circular hole. (a) Illustration of a semi-infinite plate with one semi-circular notch; (b) stress distribution $\sigma_\theta/\sigma_{max}$ with θ; (c) stress variation on $\sigma_\theta/\sigma_{max}$ with x/ρ_0; (d) illustration of an infinite plate with one circular hole; (e) stress distribution $\sigma_\theta/\sigma_{max}$ with θ for the situation in (d); (f) stress variation about $\sigma_\theta/\sigma_{max}$ with x/ρ_0 for the situation in (d).

where σ_{max} can be defined according to Fillippi et al. [44]. In addition, the relationship between σ_{max} and σ may be determined as: $\sigma_{max} = 3.06\sigma$ [45].

After substituting Eq. (3) into Eqs. (2) and (1), we can obtain the related stress expressions as follows:

$$\sigma_\theta/\sigma_{max} = \frac{1}{4}\left(\frac{\rho}{\rho_0}\right)^{-0.5}\left\{1.5\cos 0.5\theta + 0.5\cos 1.5\theta + 2.0\left(\frac{\rho}{\rho_0}\right)^{-1.0}\cos 0.5\theta\right\} \tag{4a}$$

$$\sigma_\rho/\sigma_{max} = \frac{1}{4}\left(\frac{\rho}{\rho_0}\right)^{-0.5}\left\{2.5\cos 0.5\theta - 0.5\cos 1.5\theta - 2.0\left(\frac{\rho}{\rho_0}\right)^{-1.0}\cos 0.5\theta\right\} \tag{4b}$$

$$\tau_{\rho\theta}/\sigma_{max} = \frac{1}{4}\left(\frac{\rho}{\rho_0}\right)^{-0.5}\left\{0.5\sin 0.5\theta + 0.5\sin 1.5\theta + 2.0\left(\frac{\rho}{\rho_0}\right)^{-1.0}\sin 0.5\theta\right\} \tag{4c}$$

Then, with $\rho = \rho_0$, the stress ratio of $\sigma_\theta/\sigma_{max}$ varying with θ can be illustrated in Fig. 6b. It can be seen that the maximum stress appears at the position $\theta = 0°$, along with $\sigma_\theta/\sigma_{max} = 1.0$. As θ increases, the value of $\sigma_\theta/\sigma_{max}$ displays a declining trend. In addition, in order to depict the stress value at $\theta = 0°$, Fig. 6c shows the variation in $\sigma_\theta/\sigma_{max}$ with the nondimensional distance x/ρ_0 along the x direction indicated in Fig. 6a. Here, the value of x/ρ_0 is taken as ranging from 1.0 to 3.0. The results show that the stress ratio of $\sigma_\theta/\sigma_{max}$ also presents a decreasing tendency from the edge of the notch to the interior, while the value $\sigma_\theta/\sigma_{max}$ changes from 1.0 to 0.39 with an obvious stress gradient. In addition, a similar solution can easily be derived for the hole [43]. Instead of elaborate discussions, we only display the model illustration and the related analytical

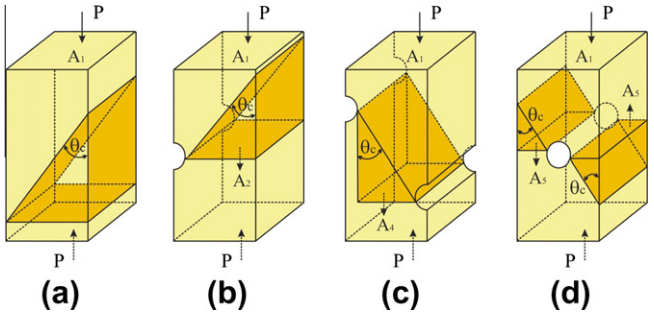

Fig. 7. Illustration of fracture behaviors for specimens A, B, D and E under compression loadings: (a) specimen without notches; (b) specimen with one notch; (c) specimen with two asymmetrical notches; (d) specimen with one circular hole.

solutions in Fig. 6d–f since the stress distributions are similar to the situation with one notch.

Therefore, in this section, the stress distributions induced by one notch or the hole are illustrated by the analytical method [43,44]. Through the above results, it can be considered that the stress concentration around the notch tips can make the SBs initiate firstly, then, on account of the stress gradient, the SBs may expand gradually until the specimens fail. Complementarily, in Section 4.2, the detailed deformation process will be simulated by FEM models.

4.1.2. Analysis of the nominal yield strength of notched specimens

4.1.2.1. Approximate analysis of specimens B, D, E. As mentioned above, specimens A, B, D and E were compressed into two parts along one major SB [11,39]. Additionally, it was found that these specimens could fracture fast with low plasticity (0.5–1.0%) once yielding started. Due to this fracture feature, the reductions in the nominal yield strengths (specimens B, D, E) can be estimated approximately.

As illustrated in Fig. 7a–d, the shear fracture modes for the four specimens above are displayed. In Fig. 7a, the specimen without notches could fail along one major SB if the stress along the loading (P) direction reaches the yield strength of 1.80 GPa. The yield strength can be computed as: $\sigma_s = P/A_1 = 1.80$ GPa [11], where A_1 is the area of top surface. The fracture mode of specimen B is illustrated in Fig. 7b. Owing to the stress concentration around the notch, the major SB might initiate from the notched region and run through the whole specimen quickly. In this situation, the effective area can be regarded as A_2 instead of A_1, as shown in Fig. 7b. Because of its low plasticity, it can be supposed that the whole specimen may fracture instantly once the stress on the effective area attains the yield strength of 1.80 GPa. Therefore, the nominal yield strength σ_n for the whole specimen with one notch can be evaluated as: $\sigma_n = \sigma_s A_2/A_1$. According to the dimensions in Fig. 2, the nominal yield strength σ_n can be obtained as: $\sigma_n = 1.50$GPa, which is in agreement with the experimental data (~1.50 GPa in Fig. 3). In a similar way, in Fig. 7c, the nominal yield strength for specimen D can be obtained as: $\sigma_n = \sigma_s A_4/A_1 = 1.20$ GPa; this value is also close to the test results (~1.25 GPa). Furthermore, we can also obtain the nominal yield strength σ_n for sample E in the same way: $\sigma_n = 2\sigma_s A_5/A_1 = 1.20$ GPa, which is very near to the experimental result (~1.25 GPa).

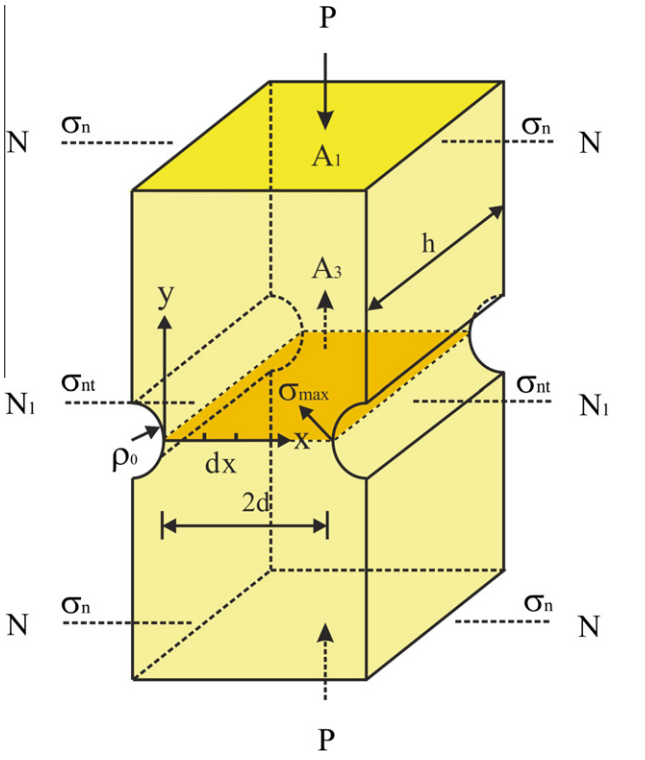

Fig. 8. Illustration of a strip with two symmetrical semi-circular notches under compression loading.

4.1.2.2. Nominal yield strength of specimen C. Unlike specimens B, D and E, for specimen C, the nominal yield strength cannot be computed by the above method since the stress in specimen C has an increasing part (the elliptical zone in Fig. 3). This implies that the yield strength should be estimated based on the global stress state in the specimen because of the large plasticity caused by the intersection of two major SBs (in Fig. 4c).

Fig. 8 shows a specimen with two symmetrical semi-circular notches under a compression loading P with the distance between two notch tips $2d$, where $\rho_0 = 0.5$, $d = 1.0$, and h is the thickness. Additionally, the nominal stress applied on the two ends of specimens (N section) can be defined as σ_n. The nominal stress on the notch tip section (N_1 section) is σ_{nt} [42,46], accompanying the maximal stress σ_{max} on the notch tips. In this loading system, the stress concentration factor K_t can be expressed as [42,46]:

$$K_t = \frac{\sigma_{max}}{\sigma_{nt}} \tag{5}$$

The approximate stress component σ_x and σ_y can be written as [46]:

$$\sigma_x = K_t\sigma_{\mathrm{nt}}\left[0.278\left(\frac{x}{\rho}\right)^{0.5} - 0.262\left(\frac{x}{\rho}\right)^{1.5} + 0.093\left(\frac{x}{\rho}\right)^{2.5} - 0.0116\left(\frac{x}{\rho}\right)^{3.5}\right] \tag{6}$$

$$\sigma_y = K_t\sigma_{\mathrm{nt}}\left[1.00 - 2.330\left(\frac{x}{\rho}\right) + 2.590\left(\frac{x}{\rho}\right)^{1.5} - 0.907\left(\frac{x}{\rho}\right)^{2.0} + 0.037\left(\frac{x}{\rho}\right)^{3.0}\right] \tag{7}$$

Therefore, the decrease in the nominal yield strength can be interpreted approximately. In Fig. 8, the average stress in the notched section (N_1 section) may be estimated by integration. With an infinitesimal dx, the stress summation Ω for σ_y on the N_1 section can be computed by integration:

$$\begin{aligned}\Omega &= 2\int_0^1 \sigma_y dx \\ &= 2\int_0^1 \left(K_t\sigma_{\mathrm{nt}}\left[1.00 - 2.330\left(\tfrac{x}{\rho}\right) + 2.590\left(\tfrac{x}{\rho}\right)^{1.5} - 0.907\left(\tfrac{x}{\rho}\right)^{2.0} + 0.037\left(\tfrac{x}{\rho}\right)^{3.0}\right]\right)dx \\ &= 1.76\sigma_{\mathrm{nt}} = 2.64\sigma_{\mathrm{n}}\end{aligned} \tag{8}$$

where $\sigma_{\mathrm{nt}} = \frac{P}{2dh}$, $\sigma_{\mathrm{n}} = \frac{P}{2(d+\rho)h}$, $K_t = 1.90$ [42,46]. Therefore, the average stress σ_a on the N_1 section can be expressed as:

$$\sigma_a = 2.64\sigma_{\mathrm{n}}/2d = 1.32\sigma_{\mathrm{n}} \tag{9}$$

Next, with regard to the global plasticity, it can be hypothesized that the whole sample may display overall plastic deformation if the average stress in the specimen σ_{aver} reaches the yield stress $\sigma_s = 1.80$ GPa. Therefore, in order to simplify problem, the average stress σ_{aver} in the whole specimen can be computed by approximately averaging the stress on the N_1 section and the N section:

$$\sigma_{aver} = (\sigma_a + \sigma_{\mathrm{n}})/2 = (1.32\sigma_{\mathrm{n}} + \sigma_{\mathrm{n}})/2 = 1.16\sigma_{\mathrm{n}}. \tag{10}$$

Hence, for the Zr-based metallic glasses in the present work, the relation between σ_{aver} and σ_s (yield stress) can be approximately estimated as:

$$\sigma_{aver} = \sigma_s = 1.80\ \mathrm{GPa},\ \sigma_{\mathrm{n}} = 1.55\ \mathrm{GPa} \tag{11}$$

Compared with the experimental results in Fig. 3, the nominal yield strength is 1.50 GPa, implying that the theoretical estimate approximates to the yield strength for specimen C.

In short, by means of different models, the reductions in the nominal yield strength caused by the notches and the hole have been discussed. Compared with the experimental results, the above results provide an approximate and simple estimation of the reductions in the nominal yield strength for the notched specimens.

4.2. Finite-element analysis

In Section 4.1, some analytical results are provided as a basis for the stress concentration caused by notches or a hole. However, such solutions were based only on elastic mechanics and did not consider the plastic deformation [42–46]. With this in mind, ideal elastic–plastic finite-element models are constructed to describe the stress distribution in the notched specimens. In the present finite-element model, a displacement control mode is established, wherein the displacement loading is exerted on one end of specimen with the other end fixed in order to describe the deformation process. Additionally, two assumptions should be pointed out: (i) concerning the yield criteria for metallic glasses [49,50], if compression yield and large plasticity are considered, the von Mises criterion is applied to the yield process of metallic glass [51]; (ii) concerning the propagation process of SBs, although the yield strength must be exceeded along the entire length of a viable shear path in order for a SB to form [52], considering the whole deformation process, we can assume that the local mature shear band (LMSB) [53] can occur in the regions where the equivalent stress has approximately reached the yield strength (1.80 GPa) because of the isotropy and brittleness of metallic glasses [41]. In Figs. 9 and 10, the red[1] regions represent the yield equivalent stress regions, implying that the SBs in these regions have formed. Moreover, compared with the simulated results, the results indicate that the SB extension process can be simulated suitably based on these assumptions.

[1] For interpretation of color in Figs. 9 and 10, the reader is referred to the web version of this article.

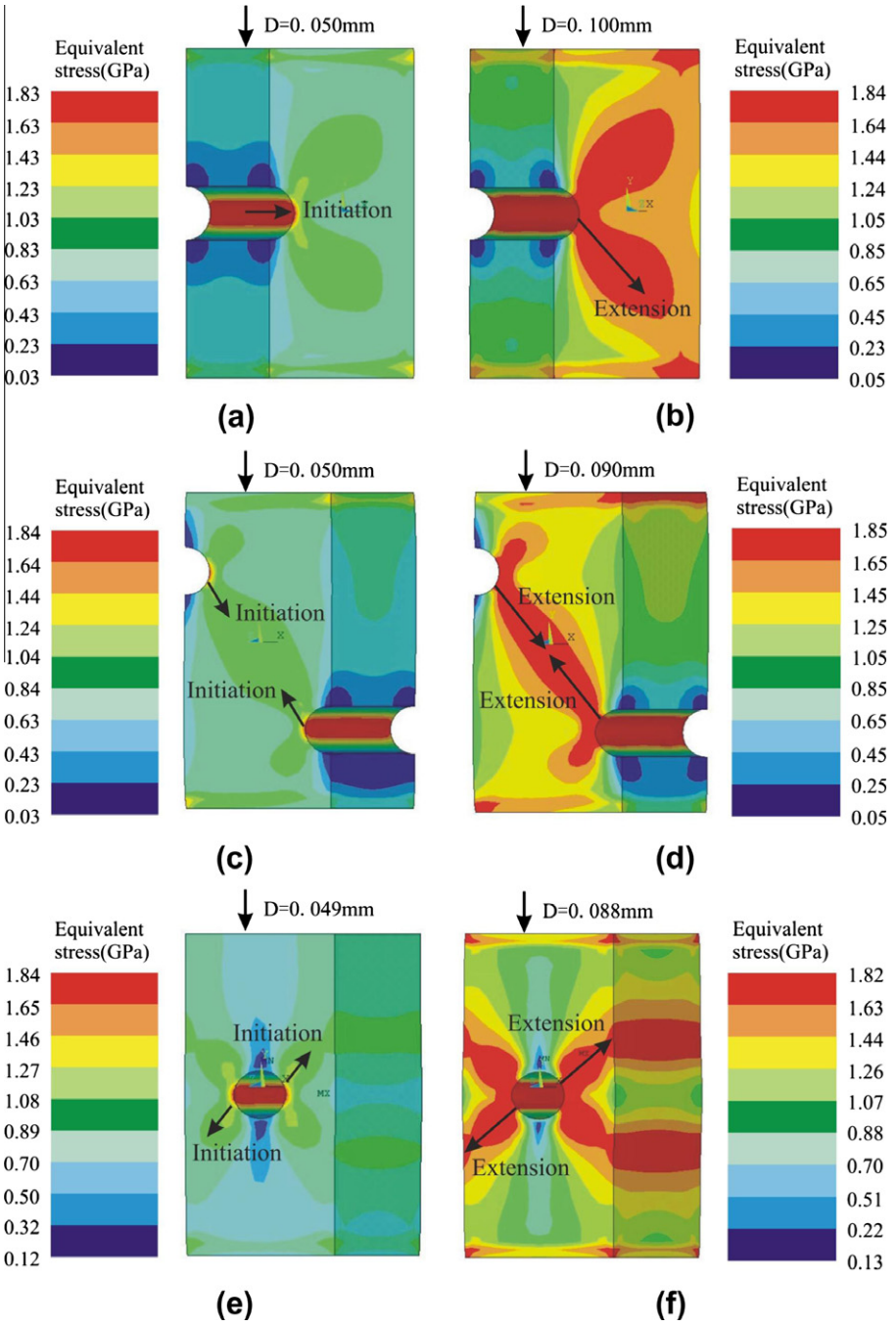

Fig. 9. Equivalent stress distributions of specimens B, D and E in Fig. 2 with different displacements: (a) 0.050 mm for specimen B; (b) 0.100 mm for specimen B; (c) 0.050 mm for specimen D; (d) 0.090 mm for specimen D; (e) 0.049 mm for specimen E; (d) 0.088 mm for specimen E. The arrows indicate the SB propagation directions and the red regions show where the local stresses have reached the yield strength. (For interpretation of the references to colour in this figure legend, the reader is referred to the web version of this article.)

4.2.1. Finite-element analysis on specimens B, D, E

The numerical results of the stress distributions for specimens B, D and E are displayed in Fig. 9a–f in which the elastic modulus of 97.8 GPa and Poisson's ratio of 0.362 were used for the Zr-based metallic glass [24,39].

First, the compression processes about specimen B are illustrated in Fig. 9a and b. In Fig. 9a, the displacement loading D applied to the specimen is 0.050 mm; in this situation, the stress around the notches has reached the yield strength and the SBs should also initiate around the notch. Then, with an increase in displacement, the SBs are found to expand from the notches to the interior of the specimen, as indicated in Fig. 9b, suggesting that the sample should rupture along the major SB with continuous increase in the displacement. In a similar way, the compression processes for specimen D with two asymmetric notches are illustrated in Fig. 9c and d. In Fig. 9c, two parallel SBs should start around the notches and subsequently roll into one major SB. When the yield stress regions run through the whole specimen, the specimen will fail along the major SB, as shown in Fig. 9d.

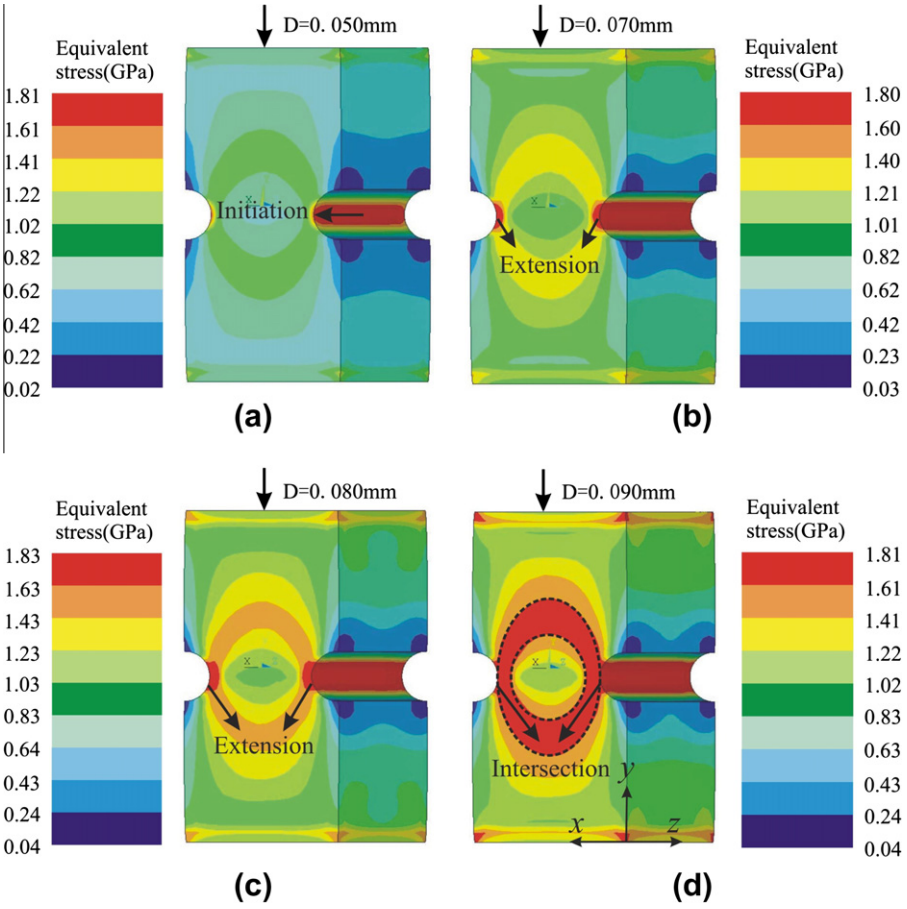

Fig. 10. Equivalent stress distribution of the specimen C in Fig. 2 with different displacements: (a) 0.050 mm; (b) 0.070 mm; (c) 0.080 mm; (b) 0.090 mm. The elliptical dashed lines represent the yield stress regions. The arrows indicate the SB propagation directions and the red regions show where the equivalent stress has reached the yield strength. (For interpretation of the references to colour in this figure legend, the reader is referred to the web version of this article.)

Similarly, the simulated results for the compression deformation processes on the Zr-based metallic glass with a hole are given in Fig. 9e and f. In Fig. 9e, the yield stress first appears in the regions around the hole, and the SBs propagate from the hole to the edges of the sample. Furthermore, with increasing displacement, as shown in Fig. 9f, the yield stress region runs through the specimen (displayed by the arrow directions in Fig. 9f), with the result that the sample can finally be broken into two parts.

Compared with the fracture behaviors in Fig. 4, the simulations for specimens B, D and E are also in agreement with the experimental results. In these situations, the major SBs can run through the entire samples instantly without high plasticity. Obviously, the key factor for the low plasticity is the lack of the confinement for the fast propagation of major SBs.

4.2.2. Finite-element analysis of specimen C

Fig. 10a–d shows the simulated results for specimen C. For Fig. 10a, the displacement loading D applied on the specimen is 0.050 mm, which yields a total compressive strain of $\varepsilon = D/L = 0.05/6.0 = 0.8\%$ (where L is the height of the specimen). In this situation, the stress around the notches should reach the yield strength even though the specimen has not yielded entirely. Then, with an increase in the displacement, in Fig. 10b and c, the SBs are found to expand from the notches to the interior of the specimen. These results are also verified by the SEM observations in Figs. 4c and 5c and d. Combined with the theoretical analysis in Section 4.1, the edge of notches should attain the yield stress and the nucleation of SBs may occur on the notch regions. Furthermore, Fig. 10d represents the situation with a displacement of $D = 0.090$ mm, which produces a total strain of $\varepsilon = D/L = 0.090/6.0 = 1.5\%$. According to the stress–strain curve in Fig. 3, the entire specimen has entered into an overall yielding deformation stage. Hence, in Fig. 10d, the yield stress region was plotted by two elliptical dashed lines and the shear deformation feature is a V-shaped pattern as obtained in Fig. 4c. This indicates that the specimen does not fracture along major SBs because the yield stress region had not run though the entire sample in the plastic deformation stage. Additionally, owing to the resistance along the y direction and the increase in the displacement, the V-shaped region could also shear along the x direction as well as the y direction, as indicated by the SEM observations in Figs. 4c and 5e. At the same time,

during the deformation process, the hydrostatic compressive stress can also help to slightly improve the plasticity since the volume of sample will shrink partly [54]. Therefore, based on the above analysis, the whole specimen is in a steady shear deformation state and displays considerable plasticity (~10%).

Therefore, compared with specimens B, D and E, installing two symmetrical notches can result in an intersection of major SBs due to the large-scale stress gradient, which can effectively confine the fast propagation of major SBs, and the entire specimen displays a considerable plasticity rather than instant fracture [11,39].

4.3. Particular shear deformation feature of metallic glass

According to the experimental results, it can be seen that the identical Zr-based metallic glass specimens with the same dimensions displayed quite different plasticity. For specimens A, B, D and E, low plasticity was found under compressive loading, accompanied by a typical shear fracture mode along one major SB [11,39], as illustrated in Fig. 4. According to the FEM simulations, the low plasticity can be ascribed to the absence of the effective restrictions on the fast propagation of a major SB. In contrast, for specimen C, the large stress gradient can make the SBs initiate easily and expand with much difficulty. Finally, the intersections of two major SBs can hinder the fast fracture of specimen and greatly improve its plasticity. Therefore, corresponding to the different geometric shapes, the metallic glass can display the various shear deformation behaviors because of the diverse stress responses.

Previously, as mentioned in Ref. [25–29], samples with smaller aspect ratios can display a larger plasticity, and this improvement in plasticity can be attributed to the instrument restriction. Although the plasticity has clearly been enhanced, in the end, the metallic glass specimen can also fail rapidly along one major SB. However, for the specimens with two symmetrical semi-circular notches in the present work, the key reason for the larger plasticity is the blocking effect of notches on the propagation of SBs. On the one hand, the two symmetrical semi-circular notches in the middle of specimen C will easily lead to the local stress concentration, which stimulates the early initiation of the local SBs around the notches. However, a specimen with a small aspect ratio has no such local stress concentration. On the other hand, once the two major SBs have formed, they should intersect with each other and their propagation would be restrained by this "intersection". Therefore, the current mechanism involving two symmetrical notches is quite different from those in Refs. [25–29].

As mentioned above, the enhancement in the plasticity of metallic glass by interaction of SBs induced by artificial

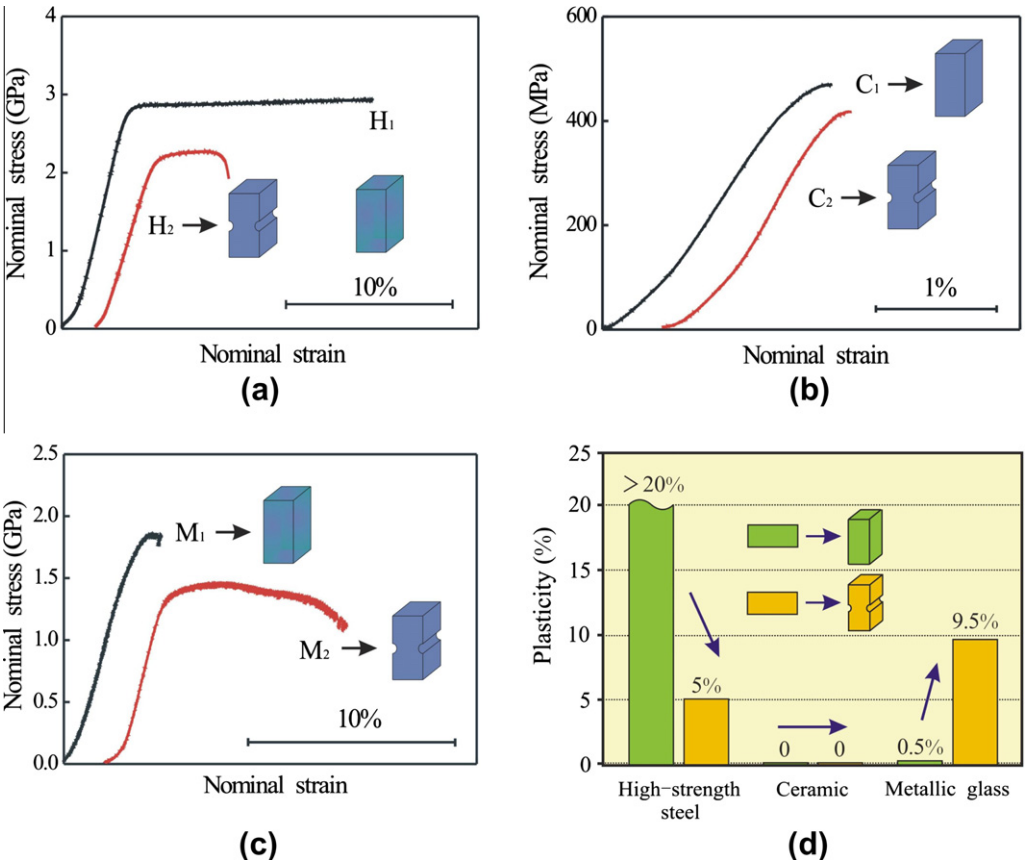

Fig. 11. Nominal compressive stress–strain curves of the specimens with or without two symmetrical notches: (a) high-strength steel material; (b) Ti_3Si_2C ceramic material; (c) Zr-based metallic glass; (d) illustration of the variations in plasticity for different materials.

notches has been verified. The method of installing notches is an approach to improving the plasticity by changing the geometric structure without affecting the essential deformation mechanism. However, not all materials can be designed in order to improve their plasticity. For comparison, we conducted similar compression tests on two other high-strength materials: high-strength steel (CM400) [55] and ceramic ($Ti_3Si_3C_2$) [56]. The results confirm that the enhanced plasticity by the artificial notches is only valid for metallic glass. In Fig. 11a, for the high-strength steel CM400 [55], the nominal compressive stress–strain curves of the samples without and with two semi-circular notches are displayed; the sample dimensions correspond with those of specimens A and C in Fig. 2. For the situation without notches, the sample has very high yield strength of about 2.8 GPa and can also display a higher plasticity of >20.0%. However, the specimen with two symmetrical notches not only displays relatively lower nominal yield strength, but also greatly decreased plasticity down to only 5.0%. Moreover, in Fig. 11b, similar compression tests were also performed on the ceramic $Ti_3Si_3C_2$ [56]. Unlike the metallic glasses, the ceramic specimen with two symmetrical notches displays zero plasticity, which is like the sample without notches. Additionally, the variation in plasticity of metallic glass caused by the artificial notches is illustrated in Fig. 11c. Obviously, as three typical materials with high strength, the specimens with two symmetrical notches may display different plastic deformations. By means of proper stress gradient, the plasticity of metallic glasses can be greatly improved, from 0.5% to ~10%; however, for the two other materials, high-strength steel and ceramics, no enhancement in plasticity enhancements is found, as illustrated for comparison in Fig. 11d. These results clearly demonstrate that the interaction of SBs induced by large stress gradients in the present work is a particular technique for improving the plasticity of metallic glasses, rather than an artificial design.

Based on the experimental results and discussion above, it is in principle suggested that the effect we have observed of an artificial notch improving the plasticity of metallic glass is similar to the yielding and work-hardening mechanisms induced by dislocations in crystalline materials (see Fig. 1b). The similarities can be summarized as follows. (i) In Fig. 1b and c, due to the dislocations in crystalline materials, the overall yield strength can be greatly decreased. Likewise, due to the stress concentration created by notches, SBs in metallic glasses initiate easily, with the result that the yield strength of metallic glass specimens can be reduced partly, as shown in Fig. 3. (ii) In Fig. 1b, in order to obtain high plasticity, the slip bands intersect with each other and the proliferation of abundant dislocations often contributes to the work hardening of the crystalline materials. Similarly, by creating two symmetrical semi-circular notches (in Fig. 2c), the intersection of major SBs is also obtained, which can effectively prevent rapid fracture of the metallic glass, as illustrated in Fig. 4c. Also, for metallic glass, abundant SBs are also found in Fig. 5e due to the intersection of major SBs, which is similar to the multiplication of dislocations in crystalline materials. As shown in Fig. 3, the intersection of the SBs should contribute to the stress increment in the stress–strain curve of the specimen C, as marked by the elliptical dashed line. In summary, the present study is the first step to applying the new idea of toughening metallic glasses through artificial macroscopic notches. These designs and results may pave a new way to improve the overall performance of metallic glasses and enhance the future application of metallic glasses as structural materials.

5. Conclusions

In view of the above experimental observations and analysis, the following conclusions can be drawn.

(1) By creating different notches on identical Zr-based metallic glass, their compressive stress–strain curves exhibit quite different features, accompanying obvious differences in their plasticity. It is interesting to find that the metallic glass specimen with two symmetrical notches can display a large plasticity up to ~10%. The plasticity improvement can be attributed to the easier initiation and the difficult propagation of the SBs. The easier initiation of SBs is due to the stress concentration around the notches; the difficult propagation is related to the intersection of two major SBs. Therefore, the specimen can display large plasticity.
(2) By performing similar tests on high-strength steel and ceramics, it is demonstrated that the plasticity enhancement by SB interaction induced by artificial notches is a particular technique for metallic glasses, and not just an experimental artifact.

Acknowledgements

The authors would like to thank Prof. Y.S. Yang and Prof. J. Shen for the technical assistance on the finite-element software and the metallic glass sample preparation, as well as the stimulating discussion with Prof. A.L. Greer and Prof. L.Z. Sun. This work was financially supported by the National Natural Science Foundation of China (NSFC) under Grant Nos. 50625103, 50871117, 50890173 and 50931005, and the National Basic Research Program of China under Grant No. 2010CB631006.

References

[1] Chen HS. Acta Metall 1974;22:1505.
[2] Spaepen F. Acta Metall 1977;25:407.
[3] Argon AS. Acta Metall 1979;27:47.
[4] Falk ML. Phys Rev B 1999;60:7062.
[5] Inoue A. Acta Mater 2000;48:279.
[6] Nieh TG, Wadsworth J, Liu CT, Ohkubo T, Hirotsu Y. Acta Mater 2001;49:2887.

[7] Yan M, Zou J, Shen J. Acta Mater 2006;54:3627.
[8] Wang G, Shen J, Sun JF, Lu ZP, Stachurski ZH, Zhou BD. Intermetallics 2005;13:642.
[9] Schuh CA, Hufnagel TC, Ramamurty U. Acta Mater 2007;55:4067.
[10] Liang WZ, Shen J, Sun JF, Wu LZ, Liaw PK. Mater Sci Eng 2008;A497:378.
[11] Zhang ZF, Wu FF, He G, Eckert J. J Mater Sci Technol 2007;23:747.
[12] Pampillo CA. J Mater Sci 1975;10:1194.
[13] Argon AS, Salama M. Mater Sci Eng 1976;23:219.
[14] Shen J, Liang WZ, Sun JF. Appl Phys Lett 2006;89:121908.
[15] Chen QJ, Shen J, Zhang DL, Fan HB, Sun JF. J Mater Res 2007;22:358.
[16] Jiang MQ, Ling Z, Meng JX, Dai LH. Philos Mag 2008;88:407.
[17] Zhao JX, Qu RT, Wu FF, Zhang ZF, Shen BL, Stoica M, et al. J Appl Phys 2009;105:103519.
[18] Hays CC, Kim CP, Johnson WL. Phys Rev Lett 2000;84:2901.
[19] He G, Eckert J, Löser W, Schultz L. Nat Mater 2003;2:33.
[20] Hofmann DC, Suh JY, Wiest A, Duan G, Lind ML, Demetriou MD, et al. Nature 2008;451:1085.
[21] Qiu KQ, Wang AM, Zhang HF, Ding BZ, Hu ZQ. Intermetallics 2002;10:1283.
[22] Choi-Yim H, Conner RD, Szuecs F, Johnson WL. Acta Mater 2002;50:2737.
[23] Lewandowski JJ, Wang WH, Greer AL. Philos Mag Lett 2005;85:77.
[24] Wang WH. J Appl Phys 2006;99:093506.
[25] Zhang ZF, Zhang H, Pan XF, Das J, Eckert J. Philos Mag Lett 2005;85:513.
[26] Bei H, Xie S, George EP. Phys Rev Lett 2006;96:105503.
[27] Sunny G, Lewandowski J, Prakash V. J Mater Res 2007;22:389.
[28] Wu FF, Zhang ZF, Mao SX. Acta Mater 2009;57:257.
[29] Han Z, Wu WF, Li Y, Wei YJ, Gao HJ. Acta Mater 2009;57:1367.
[30] Zhang Y, Wang WH, Greer AL. Nat Mater 2006;5:857.
[31] Choi YC, Hong SI. Scripta Mater 2009;61:481.
[32] Lu J, Ravichandran G. J Mater Res 2003;18:2039.
[33] Wu FF, Zhang ZF, Jiang F, Shen J, Sun J, Mao SX. Appl Phys Lett 2007;90:191909.
[34] Wu FF, Zhang ZF, Shen J, Mao SX. Acta Mater 2008;56:894.
[35] Mayers MA, Chawla KK. Mechanical behavior of materials. Upper Saddle River, NJ: Prentice Hall; 1999.
[36] Yoshida K, Goto Y, Yamamoto M. J Phys Soc Japan 1966;21:825.
[37] Obrtlik K, Robertson CF, Marini B. J Nucl Mater 2005;342:35.
[38] Bassim MN, Liu CD. Mater Sci Eng 1993;A164:170.
[39] Zhang ZF, Eckert J, Schultz L. Metall Mater Trans 2004;35A:3489.
[40] Wu FF, Zhang ZF, Shen J, Mao SX. J Mater Res 2008;23:2662.
[41] Wang WH, Dong C, Shek CH. Mater Sci Eng R 2004;44:45.
[42] Peterson RE. Stress concentration factors. New York: John Wiley; 1974.
[43] Lu MW, Luo XF. Foundation of elasticity. Beijing: Tsinghua University Press; 2001 (in Chinese).
[44] Fillippi S, Lazzarin P, Tovo R. Int J Solids Struct 2002;39:4543.
[45] Xu RX, Thompson JC, Topper TH. Fatigue Fract Engng Mater Struct 1995;18:885.
[46] Glinka G, Newport A. Int J Fatigue 1987;9:143.
[47] Kimura H, Masumoto T. Metall Trans 1983;14A:709.
[48] Flores KM, Dauskardt RH. Acta Mater 2001;49:2527.
[49] Zhang ZF, Eckert J, Schultz L. Acta Mater 2003;51:1167.
[50] Zhang ZF, He G, Eckert J, Schultz L. Phys Rev Lett 2003;91:045505.
[51] Bruck HA, Christman T, Rosakis AJ, Johnson WL. Scripta Metall Mater 1994;30:429.
[52] Packard CE, Schuh CA. Acta Mater 2007:5348–50.
[53] Shimizu F, Ogata S, Li J. Acta Mater 2006;54:4293.
[54] Lewandowski JJ, Lowhaphandu P. Philos Mag A 2002;82:3427.
[55] Wang W, Yan W, Duan QQ, Shan YY, Yu JQ, Zhang ZF, et al. Mater Sci Eng A 2010;527:3057.
[56] Zhang ZF, Sun ZM. Mater Sci Eng A 2005;408:64.